J|A|C|S
ARTICLES
Published on Web 01/15/2008

# Diffusion of Oriented Single Molecules with Switchable Mobility in Networks of Long Unidimensional Nanochannels

Christophe Jung,[†] Johanna Kirstein,[†] Barbara Platschek,[†] Thomas Bein,[†] Michael Budde,[†] Irmgard Frank,[†] Klaus Müllen,[‡] Jens Michaelis,[†] and Christoph Bräuchle*,[†]

*Department of Chemistry und Biochemistry and Center for Nanoscience (CeNS), Ludwig-Maximilians-Universität München, Butenandtstrasse 11, D-81377 München, Germany, and Max Planck Institut für Polymerforschung, Mainz, Germany*

Received August 20, 2007; E-mail: Christoph.Braeuchle@cup.uni-muenchen.de

***Abstract:*** Single dye molecules incorporated into a mesoporous matrix can act as highly sensitive reporters of their environment. Here, we use single TDI molecules incorporated as guests into hexagonal mesoporous films containing highly structured domains. The dye molecules allow us to map the size of these domains which can extend to over 100 $\mu$m. Investigation of the translational and orientational dynamics via single molecule fluorescence techniques gives structural as well as dynamical information about the host material. In an air atmosphere, the guest molecules show no movement but perfect orientation along the pore direction. The diffusion of the TDI molecules can be induced by placing the mesoporous film in a saturated atmosphere of chloroform. In single molecule measurements with very high positioning accuracy (down to 2−3 nm) the movement of molecules could be observed even between neighboring channels. This reveals the presence of defects like dead ends closing the pores or small openings in the silica walls between neighboring channels, where molecules can change from one channel to the next. A statistical analysis demonstrates that the diffusion of TDI in the mesoporous film cannot be described with a 1D-random diffusion but is more complicated due to the presence of adsorption sites in which the TDI molecules can be occasionally trapped.

## 1. Introduction

Mesoporous host materials form one of the key materials in nanotechnology, because their nanometer sized channels provide room for guest species at the molecular level.[1] Applications of these pore systems include novel drug delivery materials,[2] catalysts,[3] scaffolds for conducting nanoscale wires,[4−6] and chromatography.[7] For most of these examples a good understanding and control of the diffusion of guest molecules within the nanometer-sized channels are required. Moreover for some applications the alignment of pores on a macroscopic length-scale forming well ordered membranes is highly desirable. Recent reports address the synthesis and characterization of mesoporous host materials with an increasing degree of order of the channel systems.[8−10] In this context, the investigation and/or the control of the diffusion of guest molecules within these materials are crucial to better understand their properties in view of potential scientific and industrial utilizations.

Mesoporous materials are commonly characterized by X-ray Diffraction (XRD) and Transmission Electron Microscopy (TEM).[11−13] However, these standard techniques have some significant limitations. From XRD patterns the average pore-to-pore distances in the host system can be calculated, but information about the alignment of the pores on the substrate and on the domain structure is difficult to obtain. In contrast, TEM gives a very detailed image of the pore structure, but the areas of the sample that can be imaged are limited to a few hundred nanometers in size, and more importantly TEM imaging requires special, mostly invasive preparation, such as scratching, grinding, or ion milling. In addition, the investigation of the dynamics of guest species is not possible with these methods.

[†] Ludwig-Maximilians-Universität München.
[‡] Max Planck Institut für Polymerforschung.

(1) Laeri, F. S. F.; Simon, U.; Wark, M. *Host-Guest-Systems Based on Nanoporous Crystals: Synthesis, Properties and Applications*; Wiley VCH: Weinheim, 2003.
(2) Roy, I. O.; Tymish, Y.; Bharali, D. J.; Pudavar, H. E.; Mistretta, R. A.; Kaur, N.; Prasad, P. N. *Proc. Natl. Acad. Sci. U.S.A.* **2005**, *102* (2), 279−284.
(3) De Vos, D. E.; Dams, M.; Sels, B. F.; Jacobs, P. A. *Chem. Rev.* **2002**, *102* (10), 3615−3640.
(4) Cott, D. J.; Petkov, N.; Morris, M. A.; Platschek, B.; Bein, T.; Holmes, J. D. *J. Am. Chem. Soc.* **2006**, *128* (12), 3920−3921.
(5) Ye, B.; Trudeau, M. L.; Antonelli, D. M. *Adv. Mater.* **2001**, *13* (8), 561−565.
(6) Petkov, N.; Stock, N.; Bein, T. *J. Phys. Chem. B* **2005**, *109* (21), 10737−10743.
(7) Rebbin, V.; Schmidt, R.; Froba, M. *Angew. Chem., Int. Ed.* **2006**, *45* (31), 5210−5214.
(8) Yamauchi, Y.; Sawada, M.; Sugiyama, A.; Osaka, T.; Sakka, Y.; Kuroda, K. *J. Mater. Chem.* **2006**, *16* (37), 3693−3700.
(9) Koganti, V. R.; Dunphy, D.; Gowrishankar, V.; McGehee, M. D.; Li, X. F.; Wang, J.; Rankin, S. E. *Nano Lett.* **2006**, *6* (11), 2567−2570.
(10) Platschek, B.; Petkov, N.; Bein, T. *Angew. Chem., Int. Ed.* **2006**, *45* (7), 1134−1138.
(11) Freer, E. M.; Krupp, L. E.; Hinsberg, W. D.; Rice, P. M.; Hedrick, J. L.; Cha, J. N.; Miller, R. D.; Kim, H. C. *Nano Lett.* **2005**, *5* (10), 2014−2018.
(12) Klotz, M.; Albouy, P. A.; Ayral, A.; Menager, C.; Grosso, D.; Van, der Lee, A.; Cabuil, V.; Babonneau, F.; Guizard, C. *Chem. Mater.* **2000**, *12* (6), 1721−1728.
(13) Raman, N. K.; Anderson, M. T.; Brinker, C. J. *Chem. Mater.* **1996**, *8* (8), 1682−1701.


**10.1021/ja075927e CCC: $40.75** 

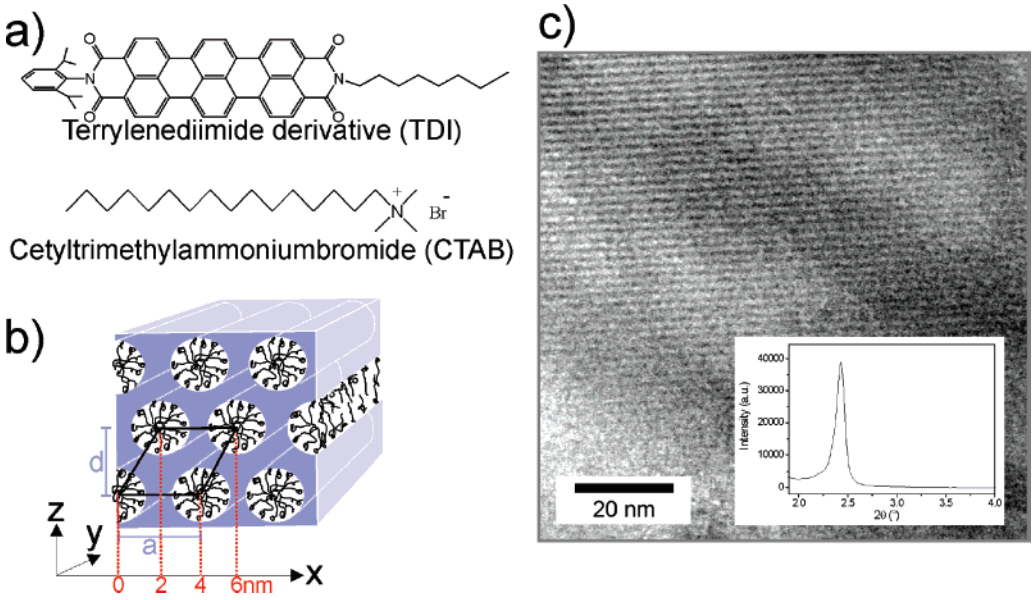


***Figure 1.*** Sample system. (a) Fluorescent terrylene diimide derivative (TDI) and structure-directing agent cetyltrimethylammoniumbromide (CTAB). The direction of the transition dipole moment of TDI is aligned with the long axis of the molecule. (b) Schematic diagram of the hexagonal mesoporous system with the arrangement of the CTAB template inside the pores. The pore-to-pore distance $a = 4.2 \pm 0.2$ nm and the layer-to-layer distance $d = 3.7 \pm 0.2$ nm are shown as well as the distances to the neighboring pores for a two-dimensional projection on the $x$, $y$ plane. (c) TEM image of the mesoporous film showing a region of parallel pores. The inset displays the small-angle X-ray diffraction pattern of the film which exhibits a strong peak corresponding to the hexagonal phase.

Ensemble diffusion of guest molecules in such materials has been studied using pulsed field gradient NMR[14] or fluorescence spectroscopic methods such as Fluorescence Correlation Spectroscopy (FCS).[15] However, a complete understanding of the dynamics of guest species inside the pores requires investigation on a molecular level.

Single Molecule Microscopy (SMM) has been established as a powerful method to resolve the individual behavior of fluorescent molecules in a wide range of systems reaching from biology[16−24] to materials science[15,25−30] and chemical processes.[31] These techniques are of great interest for the investigation of mesoporous materials, as dye molecules incorporated into host systems act as extremely sensitive molecular reporters revealing structural features of the host and information about the host−guest interactions. In this spirit we have shown how single molecules can be used as nanoscale probes to map out the structure of different topologies of mesoporous thin films.[32] Furthermore, the simultaneous observation of the orientational and spectral dynamics of the dye molecules within a CTAB-templated porous network provided direct information about the influence of the local environment on the guest molecule.[33,34]

Here we present the detailed analysis of the diffusional and orientational behavior of single terrylene diimide (TDI) dye molecules (Figure 1a) diffusing in CTAB-templated pores (2−3 nm in diameter) of hexagonal mesoporous films (Figure 1b). The films contain linear channels that are highly ordered in domains of up to 100 $\mu$m in size and can be easily mapped out with single molecule techniques. To our knowledge such a high degree of order over long distances has not been reported before.

We show the following:

(1) The diffusion of the guest molecules can be switched on and off by the surrounding atmosphere of the host/guest system. Whereas the TDI molecules are nearly immobile in an air atmosphere, they start moving as soon as chloroform vapor is added to the system.

(2) The channels dictate the direction of the diffusion as well as the orientation of the single TDI molecules; i.e., while diffusing along the porous system the molecules keep a constant orientation along the channels.

(3) The trajectories were measured with such a high spatial accuracy that the diffusion in individual channels can be resolved. The trajectories reveal the presence of defects within the mesoporous film such as dead ends or small connections

(14) Kaerger, J. *Adsorption* **2003**, *9*, 29−35.
(15) Fu, Y.; Ye, F. M.; Sanders, W. G.; Collinson, M. M.; Higgins, D. A. *J. Phys. Chem. B* **2006**, *110* (18), 9164−9170.
(16) Seisenberger, G. R.; Martin, U.; Endress, Thomas; Büning, Hildegard; Hallek, Michael; Bräuchle, Christoph. *Science* **2001**, *294*, 1929−1932.
(17) Tamarat, P. M. A.; Lounis, B.; Orrit, M. *J. Phys. Chem. A* **2000**, *104* (1), 1−16.
(18) Moerner, W. E. *J. Phys. Chem. B* **2002**, *106*, 910−927.
(19) Kulzer, F.; Orrit, M. *Annu. Rev. Phys. Chem.* **2004**, *55*, 585−611.
(20) Weiss, S. *Science* **1999**, *283* (5408), 1676−1683.
(21) Yildiz, A.; Forkey, J. N.; McKinney, S. A.; Ha, T.; Goldman, Y. E.; Selvin, P. R. *Science* **2003**, *300* (5628), 2061−2065.
(22) Shiroguchi, K.; Kinosita, K. *Science* **2007**, *316* (5828), 1208−1212.
(23) Kitamura, K.; Tokunaga, M.; Iwane, A. H.; Yanagida, T. *Nature* **1999**, *397* (6715), 129−134.
(24) Bacia, K.; Kim, S. A.; Schwille, P. *Nat. Methods* **2006**, *3* (2), 83−89.
(25) Schindler, F.; Lupton, J. M.; Muller, J.; Feldmann, J.; Scherf, U. *Nat. Mater.* **2006**, *5* (2), 141−146.
(26) Zumbusch, A.; Fleury, L.; Brown, R.; Bernard, J.; Orrit, M. *Phys. Rev. Lett.* **1993**, *70* (23), 3584−3587.
(27) Werley, C. A.; Moerner, W. E. *J. Phys. Chem. B* **2006**, *110* (38), 18939−18944.
(28) McCain, K. S. H.; David, C.; Harris, Joel M. *Anal. Chem.* **2003**, *75* (17), 4351−4359.
(29) Hellriegel, C.; Kirstein, J.; Brauchle, C.; Latour, V.; Pigot, T.; Olivier, R.; Lacombe, S.; Brown, R.; Guieu, V.; Payrastre, C.; Izquierdo, A.; Mocho, P. *J. Phys. Chem. B* **2004**, *108* (38), 14699−14709.
(30) Seebacher, C.; Hellriegel, C.; Brauchle, C.; Ganschow, M.; Wohrle, D. *J. Phys. Chem. B* **2003**, *107* (23), 5445−5452.
(31) Roeffaers, M. B. J.; Sels, B. F.; Uji-i, H.; De Schryver, F. C.; Jacobs, P. A.; De Vos, D. E.; Hofkens, J. *Nature* **2006**, *439* (7076), 572−575.
(32) Kirstein, J.; Platschek, B.; Jung, C.; Brown, R.; Bein, T.; Brauchle, C. *Nat. Mater.* **2007**, *6* (4), 303−310.
(33) Jung, C.; Hellriegel, C.; Michaelis, J.; Brauchle, C. *Adv. Mater.* **2007**, *19* (7), 956−960.
(34) Jung, C.; Hellriegel, C.; Platschek, B.; Wohrle, D.; Bein, T.; Michaelis, J.; Brauchle, C. *J. Am. Chem. Soc.* **2007**, *129* (17), 5570−5579.

between the channels. Moreover, the diffusion of the single TDI molecules is not a normal 1D random walk due to the presence of heterogeneities.

## 2. Experimental Section

**2.1. Synthesis of TDI/Mesoporous System.** The hexagonal silica films were synthesized via Evaporation-Induced Self-Assembly (EISA).[35] Samples were prepared by spin-coating precursor solutions onto cleaned glass coverslips. For the preparation of precursor solutions, 10 mmol (2.08 g) of tetraethoxysilane in 534 mmol (7.9 g) ethanol were prehydrolyzed at 60 °C for 1 h under acidic catalysis (using 3 g of 0.2 molar hydrochloric acid and 1.8 g of water). 2.00 mmol (638 mg) of cetylhexyltrimethylammoniumbromide (CTAB), the structure directing agent, in 1068 mmol (15.8 g) ethanol were added. Furthermore, terrylenediimide (TDI), a very photostable dye with a high fluorescence quantum yield[36,37] (Figure 1b), was added to the solution at an ultralow concentration ($10^{-10}$ mol/L). This precursor solution was then spin-coated onto a coverslip resulting in structured silica films with a thickness of ~120 nm (determined by ellipsometry).

The as-synthesized CTAB-templated mesoporous films with small domain sizes can be treated after synthesis to lead to more structured materials with macroscopically sized domains of almost perfectly linear channels. The observed changes are caused by a very slow reorganization of the silica matrix. A critical parameter for this process is the relative humidity (R.H.) of the atmosphere in which the samples are placed. In this study the mesoporous films were stored directly after spin-coating for ~2 weeks in an air atmosphere with a relative humidity (R.H.) of ~50%. This procedure leads to the formation of large domains (up to 100 $\mu$m in size) of linear and parallel pores. All data described in this work were measured in such domains.

**2.2. X-ray Diffractometry (XRD).** The structure of the pores in the film was determined using a Scintag XDS 2000 powder diffractometer in a $\theta/2\theta$ Bragg−Brentano scattering geometry. The mesostructured films exhibit 2D-hexagonal order; that is, the amorphous silica surrounding the CTAB-micelles forms hexagonally packed cylindrical pores parallel to the substrate (see Figure 1b and 1c, inset).

**2.3. Transmission Electron Micrographs (TEM).** The TEM images of the mesoporous films were obtained with a JEOL 2011 transmission electron microscope operating at 200 kV. For sample preparation the mesostructured film was scratched off the substrate using a razor blade; the resulting powder of mesoporous material was transferred onto an electron microscopy copper grid. A typical example is shown in Figure 1c.

**2.4. Confocal Microscopy - Orientation Measurements:** In brief, the mesoporous films were investigated with a modified inverted confocal laser scanning microscope (ZEISS LSM 410). An oil immersion objective with a high numerical aperture (ZEISS 63× 1.4 oil) and a 633 nm He−Ne laser were used for the excitation of the TDI dye molecules. For the measurement of molecular orientation, a rotating $\lambda/2$ plate was used to rotate the polarization of the excitation light.

Confocal images are acquired by scanning the excitation laser across the sample and simultaneously rotating the excitation polarization in the line-scan direction. The polarization modulation is monitored by recording simultaneously the transmitted excitation light intensity behind the sample and after a polarization filter. Details about the setup have been reported previously.[34]

**2.5. Wide-field Microscopy and Single Particle Tracking:** Fluorescence images were recorded with a wide-field setup, using an Eclipse TE200 (Nikon) epifluorescence microscope with a high numerical aperture oil immersion objective (Nikon Plan Apo 100×/1.40 N.A. Oil). The molecules are excited at 633 nm with a He−Ne gas laser with an intensity of 0.17 kW $cm^{-2}$, and their fluorescence is detected with a back-illuminated EM-CCD Camera in frame transfer mode (Andor iXon DV897, 512 px × 512 px). Incident laser light was blocked by a dichroic mirror (640 nm cutoff, AHF) and a bandpass filter (730/140, AHF). Details about the setup have been reported previously.[32]

**2.6. Data Analysis. 2.6.1. Simultaneous Measurement of Position and Orientation.** The molecule's position and two-dimensional orientation in the focal plane were determined by fitting a cosine-squared modulated two-dimensional Gaussian function to the data from a region of interest of 16 × 16 pixels centered on the molecule according to eq 1.

$$I = A_0 \exp -\frac{(x-x_0)^2}{2\sigma^2} \exp -\frac{(y-y_0)^2}{2\sigma^2} \cos^2(\omega t - \Phi_{ref} + \Phi_{mol}) \quad (1)$$

where $A_0$ and $\sigma$ are the amplitude and the width at half-maximum of the cosine-squared modulated Gaussian curve, $x_0$ and $y_0$ are the coordinates of the position of the individual molecule, $\omega$ is the angular rotation velocity of the $\lambda/2$ plate, $\Phi_{ref}$ is the phase of the modulated transmission signal (see below), and $\Phi_{mol}$ is the in-plane angle of the molecule. The zero for the angle is given by the direction of the main axis of the polarizer, which corresponds here to the horizontal line in the confocal fluorescence images.

The transmission signal was used as reference to obtain the absolute angle of the transition dipole moment. It passed through a polarizer and was recorded simultaneously to the fluorescence signal. The sum of the pixel intensity values of the horizontal lines of the region of interest was plotted versus time and was fitted with eq 1.

$$I = A_1 \cos^2(\omega t - \Phi_{ref}) \quad (2)$$

where $A_1$ is the amplitude of cosine-squared function, $\omega$ the angular speed of the $\lambda/2$ plate, and $\Phi_{ref}$ the phase of the signal.

**2.6.2. Wide-field Measurements.** The single molecule fluorescence patterns obtained were fitted by a two-dimensional Gaussian function:[38]

$$I = A_0 \exp -\frac{(x-x_0)^2}{2\sigma^2} \exp -\frac{(y-y_0)^2}{2\sigma^2} \quad (3)$$

where $A_0$ and $\sigma$ are the amplitude and the width at half-maximum of the two-dimensional Gaussian curve, and $x_0$ and $y_0$ the coordinates of the position of the individual molecule.

In order to accurately determine the position of the molecules within the porous matrix, it is important to correct for any drift in the experimental setup. We corrected for the experimentally observed drift of ~1 nm/min. To this end we first calculated the center of mass of the coordinates of bright molecules that were immobile during the observation time (e.g., 20 molecules for the trajectories shown in Figure 3b). The resulting coordinates were then subtracted from the positions of the individual TDI molecules for each frame. All the trajectories and the data analysis presented in the following are drift-corrected.

For each trajectory, a set of values for the square displacement, $\boldsymbol{r}^2(t)$, between two observations separated by the time lag $t_{lag} = n \cdot \Delta t$ (where $\Delta t$ is the time interval between successive frames of the movies, $n = 0, 1, 2, ..., N-1$ with $N$ being the total number of points in a trajectory) was computed using a custom-written LabVIEW program:

$$\boldsymbol{r}^2(t) = (\vec{r}(t + t_{lag}) - \vec{r}(t))^2 \quad (4)$$

(35) Brinker, C. J. L.; Yunfeng, Sellinger, Alan; Fan, Hongyou. *Adv. Mater.* **1999**, *11* (7), 579−585.
(36) Holtrup, F. O.; Muller, G. R. J.; Quante, H.; Defeyter, S.; DeSchryver, F. C.; Mullen, K. *Chem.−Eur. J.* **1997**, *3* (2), 219−225.
(37) Jung, C.; Muller, B. K.; Lamb, D. C.; Nolde, F.; Mullen, K.; Brauchle, C. *J. Am. Chem. Soc.* **2006**, *128* (15), 5283−5291.
(38) Gelles, J.; Schnapp, B. J.; Sheetz, M. P. *Nature* **1988**, *331* (6155), 450−453.

The Mean Square Displacements (MSDs) $\langle \boldsymbol{r}^2(t)\rangle$ for every time lag $t_{lag}$ were obtained by analyzing the distribution of the squared displacements $u$ (with $u = r^2$), which is given by[39,40]

$$p(u,t) = \frac{1}{\sqrt{2\pi(\langle r^2(t)\rangle + \sigma^2)\cdot u}} \exp\left(\frac{-u}{2(\langle r^2(t)\rangle + \sigma^2)}\right) \qquad (5)$$

where $\sigma$ corresponds to the positioning accuracy. In all the data analyses $\sigma$ was set as a fixed parameter in the fitting procedures with a value of $\sigma = 5$ nm, corresponding to the typical positioning accuracy of our data.

The cumulative probability in 1D is thus

$$P(U,t) = \int_0^U p(u,t)\, du = erf\left(\sqrt{\frac{U}{2(\langle r^2(t)\rangle + \sigma^2)}}\right) \qquad (6)$$

where *erf* is the error function, and $P(U,t)$ gives the probability that $u$ does not exceed a value $U$.

For each value of $t_{lag}$, the cumulative probability distribution $P(U,t)$ is constructed from a trajectory by counting the number of squared displacements with values $\leq U$ normalized by the total number of data points $N$. $P(U,t)$ is plotted in Figure 6a for an exemplary trajectory in a semilog scale against the squared step length $U$ for the time lag $t_{lag} = 1$ s.

A second term was added to this function in order to take into account the presence of adsorption sites in the mesoporous film where the single molecules remain immobile for a few frames.

$$P(U,t) = (1-\alpha)\cdot erf\left(\sqrt{\frac{U}{2(\langle r^2(t)\rangle + \sigma^2)}}\right) + \alpha \cdot erf\left[\sqrt{\frac{U}{2\sigma^2}}\right] \qquad (7)$$

where $\alpha$ is the weight of the population of adsorbed states in a trajectory.

**2.7. Simulations.** In order to elucidate the underlying pore structure, the experimental trajectories were modeled using three-dimensional random-walk simulations in a single layer of linear parallel pores. The random walk was confined to a pore geometry with a pore-to-pore distance of 4.2 nm. A random walk with a step length of 0.5 nm was used, and every 16 000th step was monitored in the trajectory. The intervals were chosen in order to yield an effective step length of 32 nm, in accordance with the data. Due to the nature of the undirected, statistical motion with many steps back and forth, such a high number of random walk steps is necessary to obtain the experimentally observed effective step length. A Gaussian blur with a standard deviation of $\sigma = 5$ nm was added to every point of the trajectories in accordance with experimental tracking errors. Pore geometries with linear parallel pores of different length were found to yield the best agreement with the experimental trajectories. Transitions between neighboring pores were allowed along the full pore length with a constant probability (permeability) $P$ for a random walk step that would transfer the particle from one pore to another. Values between 10% and 0.1% were chosen for the permeability $P$.

## 3. Results and Discussion

Terrylene diimide (TDI) dye molecules were incorporated into the pores of a hexagonal mesoporous thin film at very low concentration ($10^{-10}$ mol/L) to ensure that the molecules can be observed individually. Figure 1a shows the structures of TDI and the template molecule cetyltrimethylammoniumbromide (CTAB). The transition dipole moment of the TDI molecule is aligned with its long axis. Figure 1b shows a scheme of the templated hexagonal mesoporous system.

Transmission electron microscopy (TEM) images of the hexagonal mesoporous film with TDI molecules incorporated into the pores show highly ordered linear mesopores over a complete observable area of about 1.5 $\mu$m $\times$ 1.5 $\mu$m. An exemplary magnified region of about 100 nm $\times$ 100 nm is shown in Figure 1c. A typical X-ray diffractogram is displayed as an inset. The peak, in combination with the TEM image, manifests the presence of a hexagonal mesophase. From the position of the peak ($2\theta = 2.4°$) it is possible to calculate the average pore-to-pore distance $a = 4.2 \pm 0.2$ nm and a layer-to-layer distance of $d = 3.7 \pm 0.2$ nm (both indicated in Figure 1b). Typical wall thicknesses in these systems amount to about 1−2 nm;[41] thus the pore diameter is about 2−3 nm. Note here that these values vary slightly with time due to the shrinking of the mesoporous film as a result of the silica condensation.[35] Hence, all the measurements including X-ray diffractometry were performed at the same time point (15 days after synthesis). Altogether, these data show that the mesoporous films obtained are very well structured in a hexagonal phase with pores parallel over a range up to 1.5 $\mu$m. However, from these data it is not possible to obtain information about the structure on a longer length scale or on the dynamics of guest molecules inside the porous network. We used single molecule methods to overcome these limitations.

Polarization modulated confocal microscopy was performed to monitor simultaneously the diffusional and orientational behavior of the TDI molecules. Figure 2a shows a fluorescence image where single TDI dye molecules appear with a characteristic fluorescence-intensity profile (striped patterns) due to the polarization modulation during the scan. From these patterns we compute both the position of the molecule and the orientation of its transition dipole moment (shown as yellow bars; see Experimental Section for details). An immediate observation is that the transition dipole moments of all molecules have the same orientation over the whole image (about 25 $\mu$m $\times$ 10 $\mu$m). We found not only other regions with parallel aligned molecules up to 100 $\mu$m in size but also regions without preferential orientation of the molecules (data not shown). We conclude that parallel molecules indicate highly structured domains.

A time-sequence of consecutive images was recorded for the region shown in Figure 2a with 30 s per frame over a total time of about 90 min. The movie (Supporting Information, Movie 1) shows that all 95 observed molecules remain immobile with the same parallel orientation. None of the other 10 areas investigated exhibited diffusion of the fluorophores under these conditions. For all these measurements the sample was placed in an air atmosphere at 40% relative humidity (R.H.). It is known that the R.H. influences the diffusion behavior of guest molecules inside the pores.[15] We observed in other measurements (data not shown) that, at higher R.H., the molecules can diffuse very slowly in an air atmosphere. However, at very high R.H. (above 70%), the CTAB-templated films are unstable and degrade within a few hours.

We therefore looked for different conditions which would give high mobility without destroying the films during the observation time. Indeed, in a saturated chloroform atmosphere the films could be studied for several hours and the molecules were highly mobile. The three fluorescence images in Figure 2b are taken from a movie (223 frames, 30 s per frame;

(39) Anderson, C. M.; Georgiou, G. N.; Morrison, I. E. G.; Stevenson, G. V. W.; Cherry, R. J. *J. Cell Sci.* **1992**, *101*, 415−425.
(40) Schütz, G. J. S. H.; Schmidt, T. *Biophys. J.* **1997**, *73*, 1073−1080.
(41) Tanev, P. T.; Pinnavaia, T. J. *Science* **1995**, *267* (5199), 865−867.

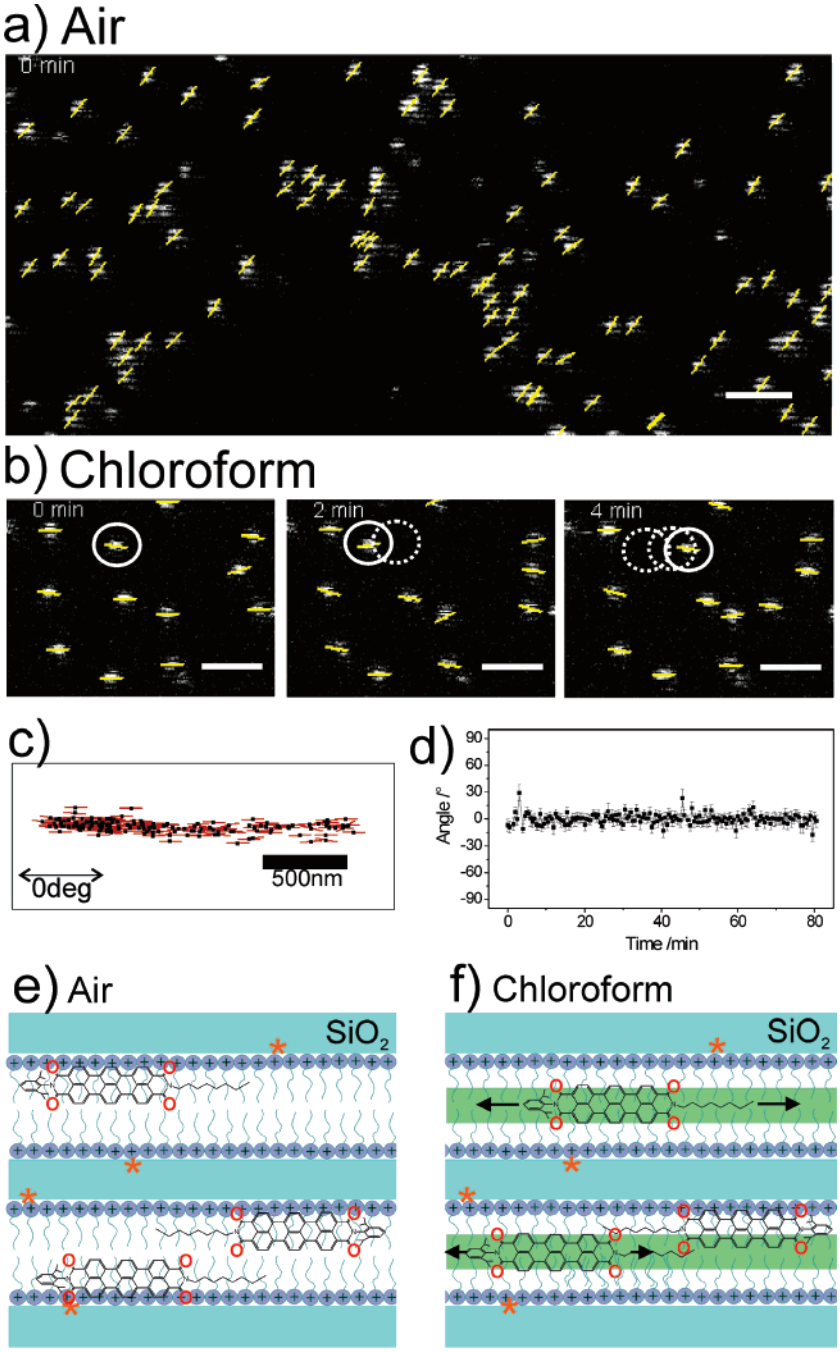


***Figure 2.*** Parallel orientation and diffusion of single TDI molecules in highly structured domains. (a) Single TDI molecules embedded in parallel pores in air atmosphere. The fluorescence image shows oriented single TDI molecules (stripped patterns); it is extracted from a time-series (Movie 1 in the Supporting Information). All visible molecules are immobile during the observation time (81 min). The determined orientations of the transition dipole moment of the molecules are depicted by yellow bars overlaid on top of the fluorescence signal. Scale bar: 2 $\mu$m. (b) Sequence of fluorescence images showing linear diffusion of single TDI molecules in a chloroform atmosphere extracted from a time series (Movie 2 in the Supporting Information). Scale bar: 2 $\mu$m (c) Trajectory extracted from the molecule marked with a white circle in (b). An animation of this trajectory is shown in Movie 3 (Supporting Information). (d) The calculated angular time trajectory of the same molecule. (e) Schematic of TDI molecules immobilized in the mesoporous material in air atmosphere. The stars indicate the presence of active silanol groups. (f) TDI molecules in the mesoporous material in the presence of chloroform. The TDI molecules are solvated (green stripe) and diffuse along the channels, and their walk is occasionally interrupted by adsorption events.

Supporting Information, Movie 2) after an observation time of 0, 2, and 4 min, respectively. The trajectory of the single TDI molecule marked with a circle in the images is displayed in Figure 2c, together with an indicator bar for its orientation. In contrast to the above measurements in an air atmosphere, diffusion of the dye molecules is observed. Moreover, as soon as chloroform is exchanged with air no more movement of the dye molecules is observed (data not shown here). This demonstrates that the diffusion of the TDI guest molecules in the porous film can be switched ON and OFF reversibly by changing the surrounding atmosphere.

The animation of this trajectory (Supporting Information, Movie 3) shows that the molecule is moving linearly back and forth over a distance of about 2 $\mu$m, while it remains remarkably aligned with the direction of the diffusion, which we assign to the direction of the pores. Figure 2d shows the time evolution

of the angle of the transition dipole moment of this molecule. The angle is constant, fluctuating slightly around a mean value of 2 ± 3°. This remarkable alignment of the fluorophores with the pores results from the tight fit of the TDI molecules (approximately 1.1 nm in diameter and 2.5 nm in length) within the nanometer sized channels (2−3 nm in diameter), preventing the TDI molecules from free rotation. Let us recall that the pores are still filled with the template used during the synthesis; thus the hydrophobic dye searches the inner part of the templated filled pores. This reduces even more the effective volume which is available for the TDI molecule. In summary, the orientation of the single TDI molecules and their trajectories map directly the direction of the channels and the domains of parallel channels.

These data show clearly the following: (i) The TDI molecules are immobile in an air atmosphere whereas they are free to diffuse in chloroform atmosphere. (ii) The diffusion is linear along the pores. (iii) The transition dipole moment does not change its orientation along the trajectories. In other words the chloroform can be used to switch on reversibly the motion of the molecules on highly structured trajectories, i.e., linear motion with constant orientation of the transition dipole moment. The immobility of the TDI molecules in an air atmosphere is most likely caused by the interactions between TDI and template molecules. The dye molecule has four oxygen atoms pointing to the side (Figure 2e) whose lone pair electrons can interact with the positively charged heads of the CTAB molecules. In addition interactions are also possible with active silanol groups or other defects in the walls of the channels.[15,42,43] In contrast, when chloroform, a good solvent for TDI, is added to the system it is likely that the small solvent molecules form a lubricant-like phase inside the pores (Figure 2f). As a result, the TDI molecules can be solvated and diffuse along the pores. Hence, the solvent exchange allows for an easy control of the diffusional behavior of the guest molecules.

Knowing that the orientation of the molecules does not change during their movement through the linear pores, we can turn to an alternative experimental technique, namely wide-field microscopy which is advantageous since much higher temporal resolution and positioning accuracy can be achieved. Series of 1000 images were acquired with a temporal resolution of 1 s per frame. Figure 3a is the overlay of an entire image series from TDI molecules embedded in a highly structured domain of the hexagonal mesoporous film and placed in an air atmosphere at 40% R.H. The single TDI dye molecules appear here as diffraction limited spots. Their positions were obtained by fitting a 2D-Gaussian function (eq 3) to the intensity profiles, and the resulting trajectories are plotted in red in Figure 3a, as an overlay on top of the sum of the 1000 fluorescence images. All molecules are immobile within our experimental accuracy. This is consistent with the results obtained with the confocal setup in an air atmosphere. Figure 3a (left inset) shows an exemplary trajectory of a TDI molecule which is found to remain immobile during the complete observation time of the movie (about 16 min). The right inset shows the histogram of a cross section along the *y*-axis. This distribution can be fitted with a Gaussian function with the standard deviation $\sigma$ = 5 nm.

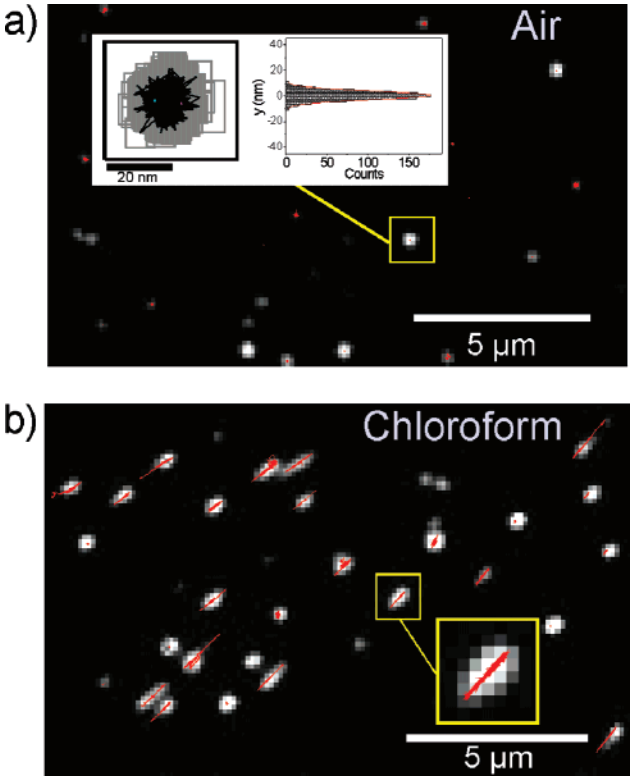


***Figure 3.*** Switching of the diffusional behavior in an air and chloroform atmosphere. (a) Overlay of 1000 wide-field fluorescence images acquired with 1 s per frame (Movie 4 in the Supporting Information; Scale bar: 5 $\mu$m) showing individual TDI molecules embedded in the mesoporous film and immobile in an air atmosphere. The single molecule trajectories are overlaid in red in the fluorescence images. The left panel of the inset displays the trace of a single, immobile TDI molecule as indicated by the yellow square. The right panel shows the histogram of the *y* cross section of the trace. The standard deviation of the distribution is $\sigma$ = 5 nm. (b) Overlay of 1000 fluorescent images acquired with 1 s per frame in a chloroform atmosphere (Movie 5 in the Supporting Information; Scale bar: 5 $\mu$m) together with single molecule trajectories (red) revealing the linear motion of TDI molecules. The linear traces map out the porous landscape of the highly structured domain. The inset is a magnification of one of the trajectories.

Figure 3b shows trajectories of molecules measured in a chloroform atmosphere. As expected, the molecules diffuse along a particular direction dictated by the orientation of the pores on an overall distance of 500−1000 nm. In order to analyze such a unidimensional trajectory it is useful to project its coordinates onto the long axis *x* of the trajectory and its perpendicular axis *y* and to analyze the new *x* and *y* coordinates separately. Figure 4a (left panel) shows an example of a linear trajectory taken from Figure 3b, and Figure 4b shows the time evolution of the $x(t)$ and $y(t)$ components. The $x(t)$ curve shows pronounced diffusion over a range of about 600 nm. Interestingly, this molecule seems to bounce back several times at the positions $x = 0$ and $x = 600$ nm and remains confined between these two extremities. This phenomenon can be attributed to "dead ends" within the porous system due to defects closing the pores at specific locations. In contrast, there is very little movement in the direction perpendicular to the trajectory. The histogram of the $y(t)$ values shown in Figure 4b can be fitted by a Gaussian function. Although the amplitude of the fluorescence signal obtained by the fit is about 20% higher than that for the immobile molecule mentioned above, indicating an even higher positioning accuracy, the standard deviation $\sigma$ =

(42) Nawrocki, J. *J. Chromatogr. A* **1997**, *779* (1−2), 29−71.
(43) Cox, G. B. *J. Chromatogr. A* **1993**, *656* (1−2), 353−367.

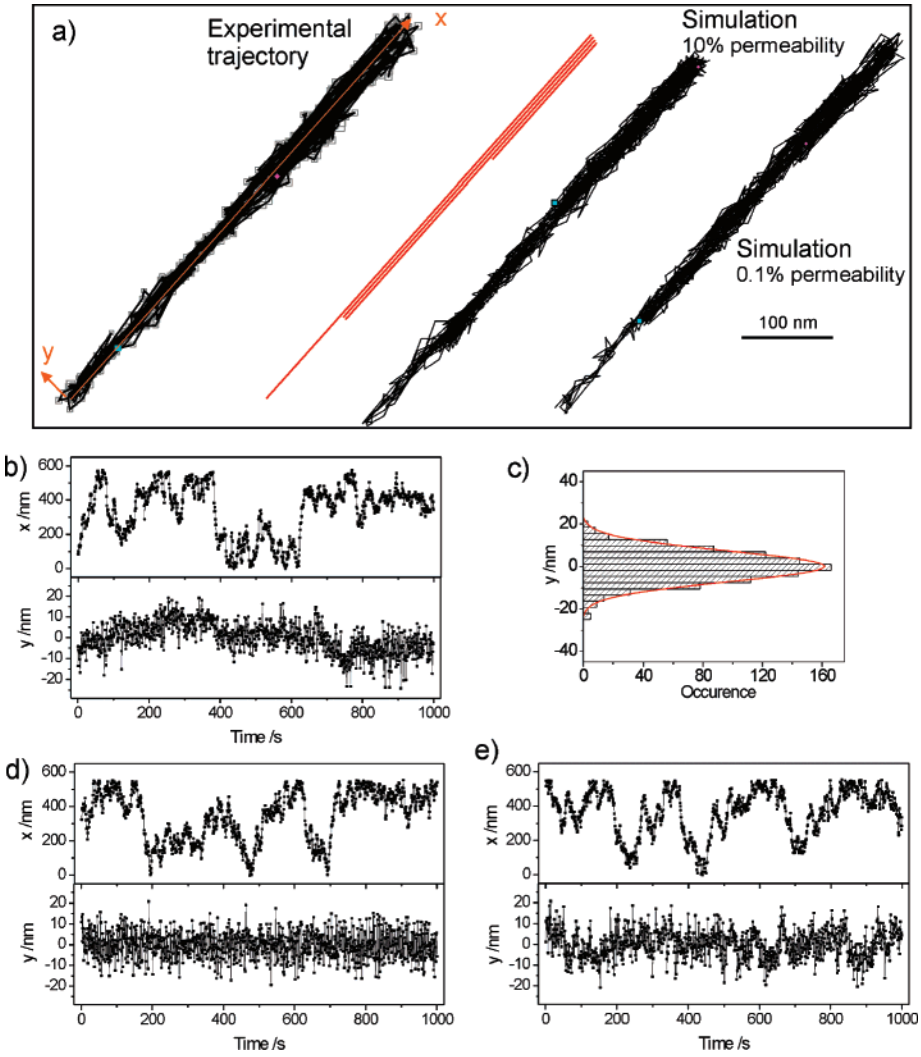


***Figure 4.*** Diffusional analysis of an individual trajectory. (a) From the left to the right: experimental trajectory, model of the geometry of the pores, and simulated trajectories with 10% and 0.1% permeability between neighboring pores, respectively. (b) Projected coordinates onto the long axis of the experimental trajectory (*x*, upper panel) and onto the transversal axis (*y*, lower panel) versus time. (c) Histogram of the *y* transversal coordinates together with a Gaussian fit. The standard deviation is $\sigma = 7$ nm. (d and e) Projected *x* and *y* coordinates for the simulated trajectories with 10% and 0.1% permeability, respectively.

7 nm now is slightly higher (compared with $\sigma = 5$ nm for the immobile molecules). This suggests that the diffusion of this TDI molecule does not occur in a single channel but in a few parallel ones. Thus, connectivity between the channels has to be assumed, which can be explained by the presence of small defects within the silica walls of the pores through which the dye molecule occasionally escapes to a neighboring channel. Let us note here that the whole section of the mesoporous film (~120 nm of thickness as measured by ellipsometry) is in the focus of the laser spot (>1 $\mu$m in size along the optical axis). Thus, all jumps between neighboring channels in the *xy* plane as well as in the *z* direction can occur and should show abrupt jumps of about 2, 4, or 6 nm (see the projections of the pore centers onto the *x*-axis in Figure 1b). However, as these values are on the same order or smaller than our positioning accuracy, it is not possible to determine the exact number of pores in which the molecule moves.

To better understand the observed dynamics of the TDI molecules, we performed simulations using a 3D random walk model of a particle diffusing in a single layer of parallel channels with a pore diameter of 4.2 nm and an effective average step length of 32 nm. The model of the geometry of the pores in which the molecule can diffuse was adapted in order to match the shape of the experimental trajectory and is displayed to its right in Figure 4a. Moreover, a certain permeability of the pore walls due to the presence of defects in the silica walls was taken into account. Two simulated trajectories are displayed to the right in Figure 4a with a permeability of 10% and 0.1%, respectively.

Such a constant permeability represents the simplest approximation and does not take into account heterogeneities neither within the silica structure nor in the template. At first sight both of the simulated trajectories resemble the data. However, a closer comparison between simulation and experiment can be drawn by looking at the *x* and *y* time trajectories displayed in Figure 4d and 4e for the simulations with 10% and 0.1% permeability, respectively. The $x(t)$ graphs of the two simulated curves show similar confined diffusion with 1D back and forth movement of the particle. This is different for the $y(t)$ graph. Whereas the $y(t)$ graph of the simulation with high permeability (10%) shows fluctuations around a mean value, the $y(t)$ graph with lower permeability (0.1%) exhibits a stronger tendency to plateaus, which is in better accordance with the experimental data. Therefore we conclude that the lower

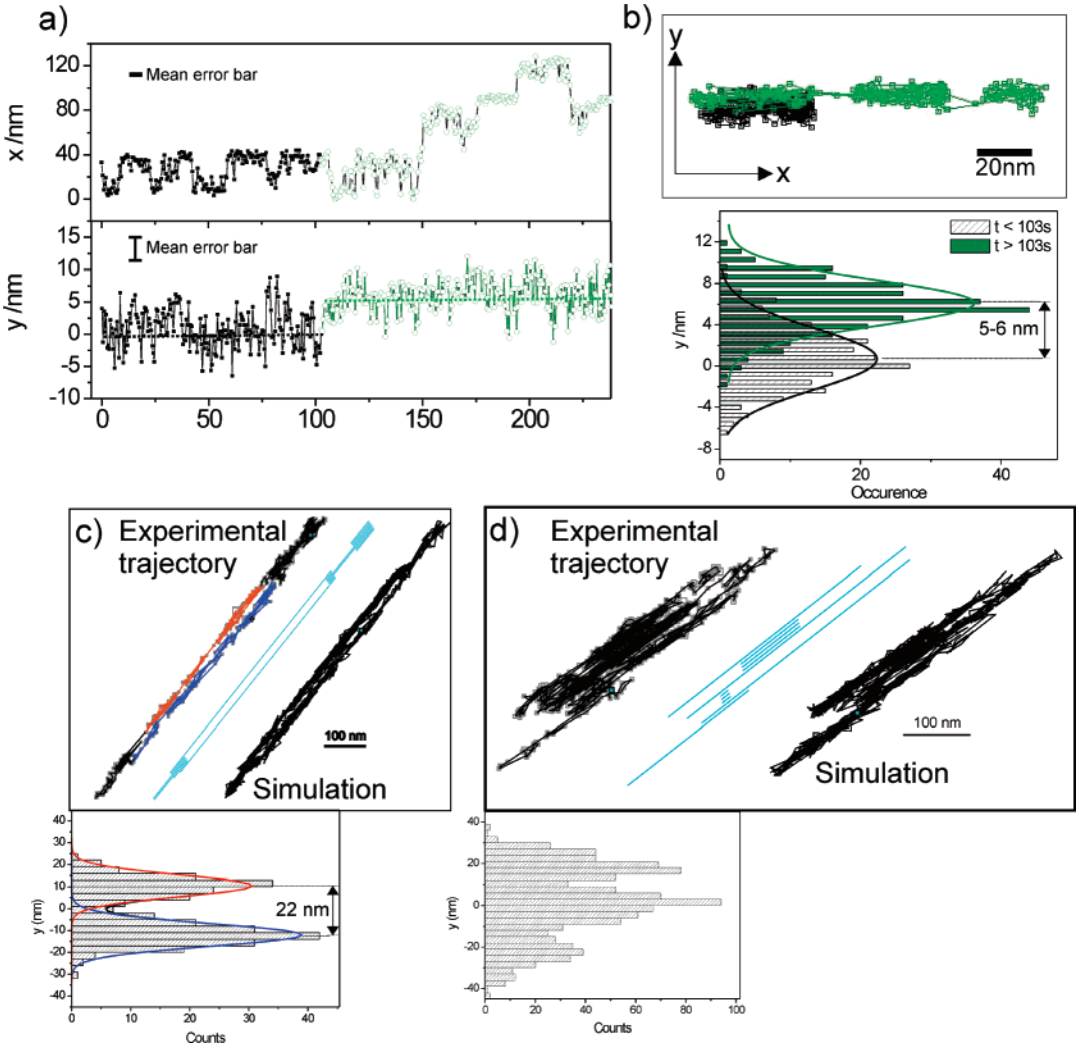


***Figure 5.*** Diffusion through defects in the silica pore walls. (a) Projected $x$ and $y$ coordinates for a single TDI molecule diffusing at least in two distinct neighboring pores. While in the first 103 s the molecule diffuses back and forth in one pore (black squares), it then switches to another pore, where it presumes its lateral diffusion (green circles). (b) Trajectory of the molecule (top) and histograms of the $y$ lateral coordinate for the time intervals before (black striped bars) and after (green full bars) the time $t = 103$ s together with their Gaussian fits (bottom). The two maxima are separated by 5−6 nm. An animation of this trajectory is shown in Movie 6 in the Supporting Information. (c) Trajectory showing the diffusion in parallel pores. From the left to the right: experimental trajectory, the model of the pores used for the simulation, and the simulated trajectory. The lower panel shows the histogram of the lateral $y$ coordinates in the middle part of the trajectory (red and blue points in the experimental trajectory). An animation of this trajectory is shown in Movie 7 in the Supporting Information. (d) Diffusion in a region rich in defect sites. The lower panel shows a diagram of the linear diffusion in the long unidimensional channels. Transition between neighboring channels can occur through small defects within the silica structure.

permeability is the more realistic description of the observed diffusion. These results suggest that it is possible to simulate the experimental trajectory on the basis of a simple model and that the defect density along the pores has to be relatively low to lead to rare transitions between pores. Note, however, that the experimental trajectories are not detailed enough to discriminate clearly between a constant permeability along the full length of the pores and jumps at discrete defect sites.

In order to observe more accurately jumps between neighboring pores we performed measurements using a 3-fold higher laser power (0.50 kW cm$^{-2}$ at the entrance of the objective). The obtained trajectories are shorter in time due to faster photobleaching, but higher temporal resolutions (500 ms/frame) as well as higher spatial resolutions ($\sigma = 2-3$ nm for the brightest molecule) could be achieved. Figure 5a shows the $x(t)$ and $y(t)$ graphs obtained from the tracking of a single TDI molecule diffusing in only a few neighboring channels (trajectory shown in Figure 5b, top). By inspection of the $y(t)$ graph this trajectory can be divided into two distinct parts which are the time intervals before (black) and after (green) 103 s. Figure 5b displays the histograms of $y(t)$ before (green full bars) and after (black dashed bars) 103 s. These distributions are clearly distinct and can be fitted by two Gaussian curves with a maximum at 0.6 and 6.1 nm and with $\sigma = 2.9$ and $\sigma = 2.3$ nm, respectively. We attribute these dynamics to a molecule switching between at least two pores separated by 5−6 nm.

The $x(t)$ graphs in Figure 5a show a back and forth movement of the molecule which remains clearly confined between $x = 0$ and $x = 40$ nm during the first 150 s of the trajectory. At this time, the molecule finds its way out of this confined region and is able to diffuse further.

The experimental trajectories described above reveal a certain connectivity between fairly close channels. In some cases the molecule can even explore much more distant pores. This is illustrated by the trajectory shown in Figure 5c. Here the single molecule diffuses in clearly separated parallel channels. The

animation of this trajectory (Movie 7 in the Supporting Information) shows that the molecule spends the first 340 s in the upper right part of the trajectory where it undergoes strong longitudinal and transversal diffusion. After this period, it suddenly finds its way out of this region (within below 1 s, our temporal resolution) and moves more rapidly to the lower left part of the trace where it remains during the next 100 s. Finally the fluorophore diffuses up again following another distinct parallel channel until it photobleaches. The histogram displayed below in Figure 5c shows the distribution of the $y(t)$ values within the time intervals in which the molecule diffuses in the middle part of the trajectory. Two Gaussian distributions can clearly be distinguished, with their maximum separated by 22 nm. This value corresponds to about six channels. The standard deviations of the single peaks are each ~5 nm, which corresponds to our positioning accuracy for this particular molecule. This analysis confirms that the molecule does not diffuse in a single channel but in parallel pores which are interconnected by small defects in the structure.

Moreover, we observed that the density of such nanodefects can vary within the same highly structured domain. Figure 5d is an example of a trajectory where a strong lateral diffusion occurs with an overall amplitude of about 70 nm in the lateral direction. The corresponding histogram of the $y$ coordinates (below Figure 5d) shows a broad distribution where several peaks can be observed. Here the dye molecule frequently jumps from one pore to another revealing the presence of a region rich in defect sites.

Similar to the trajectory described in Figure 4, the two trajectories discussed above could be simulated. The right parts of Figure 5c and 5d show the channel structures used for the simulations as well as the simulated trajectories. This shows that even for regions where defect sites occur more frequently the observed data can be described fairly well with our simulations.

Up to this point we have shown that the study of the diffusion of single TDI guest molecules gives structural information about the host material because it allows mapping out the structure of the porous network in great detail. Moreover, it reveals the presence of defects such as dead ends or small openings within the porous system.

Additional insight can be gained about the interactions between the guest molecule and the host matrix. For instance, by inspecting the $x(t)$ and $y(t)$ time trajectories one can notice the presence of time intervals during which the molecule seems to remain immobile. In Figure 5a, for example, both $x(t)$ and $y(t)$ remain constant between $t = 176$ s and $t = 194$ s, suggesting that the molecule is immobilized (within our positioning accuracy). This means that the molecule is occasionally trapped at some sites along its trajectory. We interpret this "stop and go" movement as the influence of adsorption sites. We have seen in the discussion of Figure 2e,f that interactions with the cationic heads of the template molecules or with defect sites are two likely causes for the observed adsorption in an air atmosphere, leading to an immobilization of the TDI molecules. In the presence of chloroform these interactions also have an influence on the diffusion of the guest molecules, which can be resolved with the higher time resolution of the wide-field experiments. However, the strength of these interactions is reduced by the lubricant-like behavior of chloroform, and therefore the TDI molecules are only occasionally immobile. Such an adsorption could occur if the TDI molecules escape from the shell of chloroform and interact directly with the charged head groups of CTAB. Similar diffusional behavior has been reported previously for other adsorbates diffusing at silica surfaces both at the ensemble and at the single molecule level. For example, cationic dioctadecyl-tetramethylindocarbocyanine perchlorate (DiI) dye molecules[44,45] as well as nucleotides[46] were monitored at a chromatographic interface of chemically modified fused silica. Higgins et al. have investigated the diffusion of Nile Red dye molecules in CTAB-templated as well as in calcined mesoporous films.[15] In this study it was concluded that the lateral transport of the molecules is described by fast lateral diffusion interrupted by rare, reversible adsorption to defect sites. It was postulated that strong adsorption occurs at active silanols via hydrogen bonding to the quinonal oxygen of Nile Red. In our experiments a third physical explanation for the immobilization of the guest molecule may be the presence of pores with a smaller diameter. Indeed, the X-ray micrograph (Figure 1c, inset) shows the presence of a peak at $2\theta = 2.4°$, which is relatively broad. One explanation of the broadening of the peak is that the pore diameters are not perfectly uniform but exhibit a broad distribution. Since the interior diameter of the pores is only slightly larger than the diameter of the TDI molecules, a small reduction of the diameter could already have a drastic effect on the diffusion of the molecules, thus leading to an adsorption site.

To investigate quantitatively the diffusion of TDI in the mesoporous film and to evaluate the influence of the adsorption sites on the diffusion in the presence of chloroform we have performed a statistical analysis of the linear trajectories of about 80 single TDI molecules. A first intuitive and straightforward model for the diffusion in such linear pores is a 1D random diffusion along the $x$-axis. The analysis of this diffusion was based on the cumulative probability distributions of the squared displacements. Compared with the standard method of the Mean-Square Displacement (MSD), the use of the cumulative probability distributions greatly increases the information of mobility studies, allowing us to resolve more complex behavior, including the effect of local heterogeneities within the sample. Figure 6a shows the probability distribution of the squared displacements where the probability of every step is plotted against the squared step for time lags of 1 s. In the case of a one-dimensional random walk this distribution should be described by an Error Function (eq 6 in the Experimental Section).

The red dashed line is the fit of eq 6 to the data ($\chi^2 = 7.4 \times 10^{-4}$). It is obvious that a 1D random walk model is not an accurate enough model to describe the observed diffusion. The gray dotted line shows the fit using a linear combination of a 1D random walk and a second term which takes into account the presence of adsorbed states (eq 7, for details see Experimental Section). This model describes the data better, and the chi-squared of this fit ($\chi^2 = 9.1 \times 10^{-5}$) is 8-fold reduced compared to the fit using eq 6, which justifies the use of additional terms. The determined fit parameters are the mean squared displacement $\langle \boldsymbol{r}^2(1s) \rangle = 1470$ nm$^2$/s, and the weight of the population of adsorbed states $\alpha = 13\%$. In other words,

(44) Wirth, M. J. S.; Derrick, J. *Anal. Chem.* **1998**, *70* (24), 5264−5271.
(45) Wirth, M. J. S.; Derrick, J.; Ludes, Melody, D. *J. Phys. Chem. B* **2003**, *107*, 6258−6268.
(46) Wirth, M. J. S.; Derrick, J. *J. Phys. Chem. B* **2001**, *105*, 1472−1477.

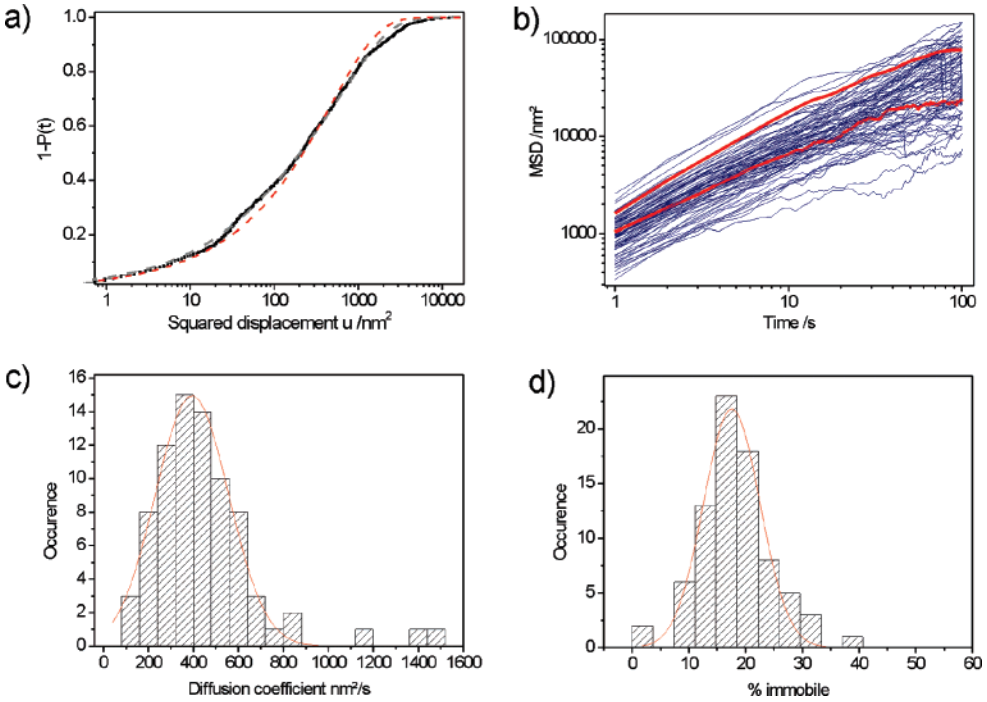


***Figure 6.*** Statistical analysis of the diffusion. (a) The cumulative probability distribution $P(u,1\text{ s})$ for a time lag $t_{lag} = 1$ s for the trajectory shown in Figure 4. The separation of the 1D diffusion and the adsorbed states is obtained by a statistical evaluation of squared step lengths (see text for details). (b) Mean squared displacement of the linear diffusion as a function of time. The upper red thick line corresponds to the trajectory displayed in Figure 4. The lower red thick line is an example of confined diffusion due to the presence of "dead ends" closing the pores at specific locations. (c) Histogram of the diffusion coefficients $D$ extracted from the MSD plots. The distribution can be fitted with a Gaussian function with a mean diffusion coefficient of 390 nm$^2$/s. (d) Histogram of the percentage of adsorbed states in a trajectory for a time lag of $t_{lag} = 1$ s. The red line is the Gaussian fit with a mean adsorption time per trajectory of 18%.

during its whole walk and for a time lag of $t = 1$ s the TDI molecule is on average 13% of the time immobilized at adsorption sites and diffuses the rest of the time with a 1D random walk. The percentage in time of adsorption clearly depends on the time resolution of the measurements (1 s per frame in this case) and decreases with higher time lags. All the other trajectories could be described well by this model, confirming the presence of adsorption sites distributed over all the mesoporous film. The same procedure was applied for time steps of 2 s, 3 s, up to 100 s. The resulting MSDs (corresponding to 10% of the total acquisition time of the trajectory) are plotted versus time for 80 molecules in Figure 6b. Most of these plots are not perfectly linear as it would be expected for a normal random walk but are slightly curved for high time values. This indicates the presence of a confined diffusion, which is consistent with the presence of "dead ends" in the structure already mentioned above. However, the MSD graphs are approximately linear for the first 10 points, and it is possible to extract a diffusion coefficient using the relationship between MSD and time for a random walk in one dimension:

$$MSD = \langle \mathbf{r}^2(t) \rangle = 2 \cdot D \cdot t \qquad (8)$$

where $D$ is the diffusion coefficient.

The distribution of the diffusion coefficients for the 80 trajectories is shown in Figure 6c. It resembles a Gaussian curve with a mean diffusion coefficient of 390 nm$^2$/s. Figure 6d displays the histogram of the percentage of adsorption time per trajectory for a time lag of 1 s. The distribution is also a Gaussian with a maximum at 18% of the time, which means that a molecule spends on average 18% of its walk immobilized at an adsorption site.

An additional interesting observation is that the distributions are both really broad which denotes the presence of large heterogeneities.

## 4. Conclusion

In summary, the diffusion of TDI molecules in the mesoporous films was investigated with a precision down to the single-channel limit, and the rich information obtained can be divided into two classes:

(1) structural information about the mesoporous silica structure: highly linear channels at micrometer length scale and the presence of rare defects in the structure such as "dead ends" where the pores are closed, or small connections between the pores.

(2) information about the dynamics of guest species: the overall diffusion process can be described by a 1D random walk interrupted occasionally by time intervals where the molecule is trapped at adsorption sites.

The increasing ability to orient mesostructured materials on a macroscopic length scale opens the possibility to exploit the organization of mesoporous solids for applications in which ordered, anisotropic, or even monolithic structures are required. Promising applications include separations, catalysis, chemical sensors, and host−guest chemistry. The methodology presented here is a valuable tool to characterize large structured areas of such mesoporous films. In particular, rich and detailed information can be gained about defects within the structure, which, for example, is of paramount importance for optimizing the synthesis procedure for highly structured molecular membranes for molecular sieving.

**Acknowledgment.** This project was funded by the SFB 486, the SFB 749, and the Nanosystems Initiative Munich (NIM).

**Supporting Information Available:** Movie 1: Oriented and immobilized single TDI molecules in a mesoporous film in air atmosphere. The orientations of the transition dipole moment are depicted by yellow bars. The images were acquired with 30 s per frame. Scale bar: 2 $\mu$m. Movie 2: Single TDI molecules diffusing in a mesoporous film in chloroform atmosphere. Images were acquired with 30 s per frame. Scale bar: 2 $\mu$m. Movie 3: Animation of the trajectory of a TDI molecule diffusing linearly in chloroform atmosphere. Movie 4: Wide-field movie of individual TDI molecules in a mesoporous film in air atmosphere. Images acquired with 1 s per frame. Scale bar: 5 $\mu$m. Movie 5: Wide-field movie of single TDI molecules diffusing in a mesoporous film in chloroform atmosphere. Images acquired with 1 s per frame. Scale bar: 5 $\mu$m. Movie 6: Animation of the trajectory of a single TDI molecule diffusing in two distinct neighboring pores. Images acquired with 0.5 s per frame. Scale bar: 20 nm. Movie 7: Animation of the trajectory of a TDI molecule diffusing in parallel pores. Images acquired with 1 s per frame. Scale bar: 100 nm.

JA075927E